

Site engineering strategy toward enhanced luminescence thermostability of Cr³⁺ doped broadband NIR phosphor and its application

Shengqiang Liu, Hao Cai, Shiyou Zhang, Zhen Song, Zhiguo Xia, Quanlin Liu*

The Beijing Municipal Key Laboratory of New Energy Materials and Technologies, School of Materials Sciences and Engineering, University of Science and Technology Beijing, Beijing 100083, China.

* Corresponding Author: E-mail address: qlliu@ustb.edu.cn (Quanlin Liu)

Table S 1. The refined structural parameters of SGO with P $6_3/mmc$.

Atom	x	y	z	Occ.	Site	space group	P $6_3/mmc$ (194)	
1 Ga	Ga ^I	0.000(0)	0.000(0)	0.000(0)	1.000	2a	symmetry Lattice parameters (\AA)	hexagonal $a=5.793(0)$ $c=22.819(1)$
3 Ga	Ga ^{II}	0.000(0)	0.000(0)	0.242(7)	0.500	4e		
4 Ga	Ga ^{III}	0.333(3)	0.666(7)	0.027(4)	1.000	4f		
6 Ga	Ga ^{IV}	0.333(3)	0.666(7)	0.190(1)	1.000	4f		
7 Ga	Ga ^V	-0.168(5)	0.163(1)	0.109(5)	1.000	12k		
8 O	O ^I	0.000(0)	0.000(0)	0.150(7)	1.000	4e		
9 O	O ^{II}	0.666(7)	0.333(3)	0.055(3)	1.000	4f	R_p	7.101
10 O	O ^{III}	0.181(8)	-0.181(8)	0.250(0)	1.000	6h	R_w	9.413
11 O	O ^{IV}	0.155(5)	-0.155(5)	0.052(5)	1.000	12k	R_{exp}	4.219
12 O	O ^V	0.504(5)	-0.504(5)	0.150(0)	1.000	12k		
13 Sr	Sr ^I	0.666(7)	0.333(3)	0.250(0)	1.000	2d		

Table S 2. Ga-O bond length data derived from refined results.

	Bond length (\AA)	Average (\AA)		Bond length (\AA)	Average (\AA)		Bond length (\AA)	Average (\AA)
Ga ^I -O	1.967(1)	1.967		1.944(7)			2.073(5)	
	1.967(1)			2.046(3)			1.923(4)	
	1.967(1)		Ga ^{IV} -O	1.944(7)	1.996		1.874(7)	
	1.967(1)			2.0463)			2.073(5)	1.979
	1.967(1)			2.046(3)			1.874(4)	
	1.967(1)			1.944(7)			2.056(2)	

Table S 3. Photoluminescence properties of some Cr^{3+} doped shott.

Host	E_m (nm)	IQE (%)	EQE (%)	$I_{500\text{K}}$ (%)	Refs
LiScP_2O_7	877	38	20	< 20	S1
$\text{LaSc}_3(\text{BO}_3)_4$	850	23	~	< 30	S2
ScBO_3	800	72.8	~	~	S3
$\text{La}_2\text{MgZrO}_6$	825	58	~	< 40	S4
$\text{Ca}_2\text{LuZr}_2\text{Al}_3\text{O}_{12}$	760	69.1	31.5	40	S5
$\text{Ca}_2\text{LuScGa}_2\text{Ge}_2\text{O}_{12}$	800	53	~	< 40	S6
$\text{Ca}_3\text{Sc}_2\text{Si}_3\text{O}_{12}$	~770	92.3	25.5	90	S7
$\text{Y}_2\text{CaAl}_4\text{SiO}_{12}$	744	75.9	~	< 80	S8
$\text{SrGa}_{12}\text{O}_{19}$	770	98.2	45	86.5	This work

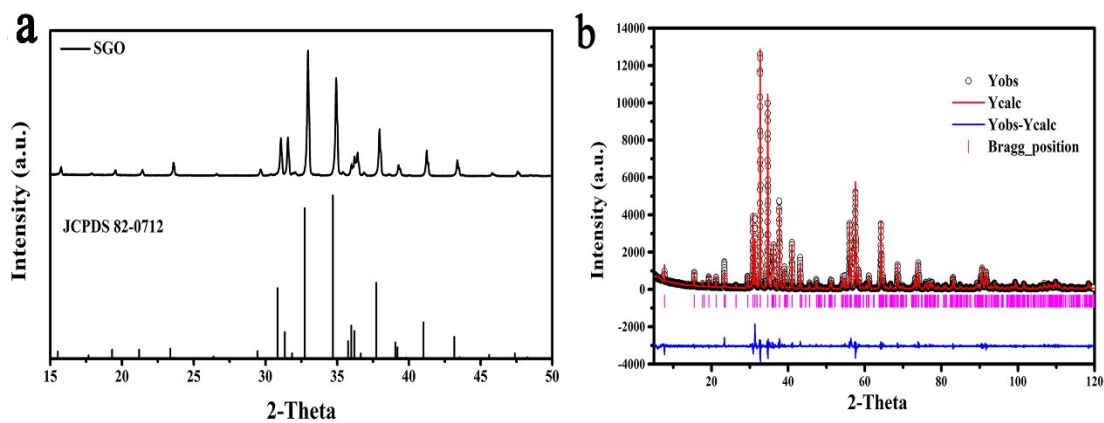


Figure S1. (a) XRD patterns of un-doped SGO and standard Bragg reflection peaks of JCPDS 82-0712. (b) Rietveld refinement result of un-doped SGO.

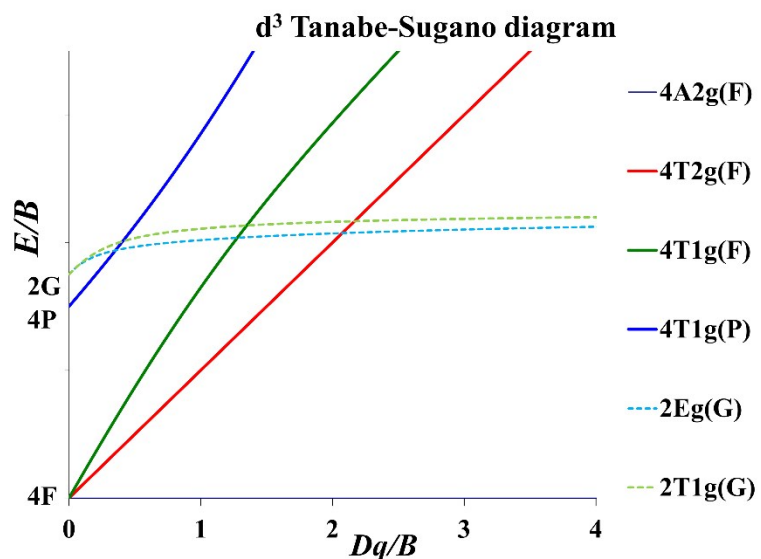


Figure S2. Tanabe—Sugano energy-level diagram for Cr^{3+} ($[\text{Ar}]3\text{d}^3$) in SGO host.

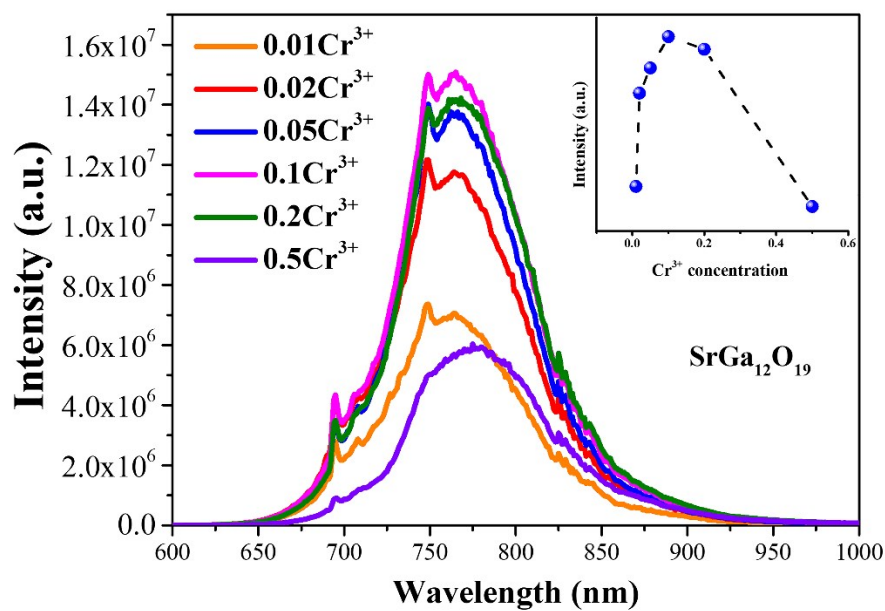


Figure S3. Concentration-dependence PL spectra for $\text{SrGa}_{12-x}\text{O}_{19}:x\text{Cr}^{3+}$ ($x=0.01, 0.02, 0.05, 0.1, 0.2, 0.5$). The inset shows the integrated intensity vs Cr^{3+} concentration scatters.

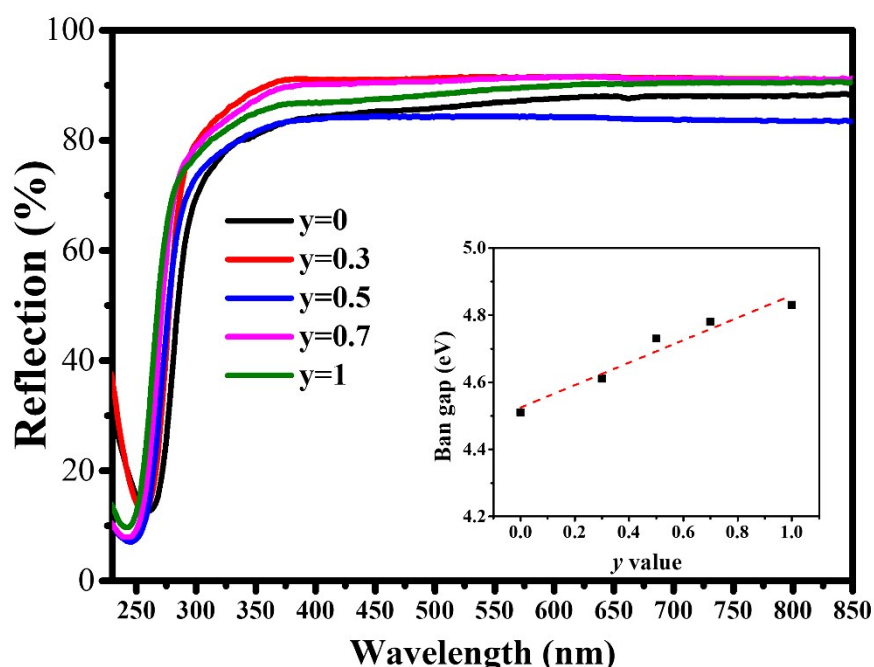


Figure S4. UV diffuse reflection spectra for the solid solution $(\text{SrGa})_{1-y}(\text{LaMg})_y\text{Ga}_{11}\text{O}_{19}$. ($y=0-1$). The inset shows the bandgap (eV) as a function of y value.

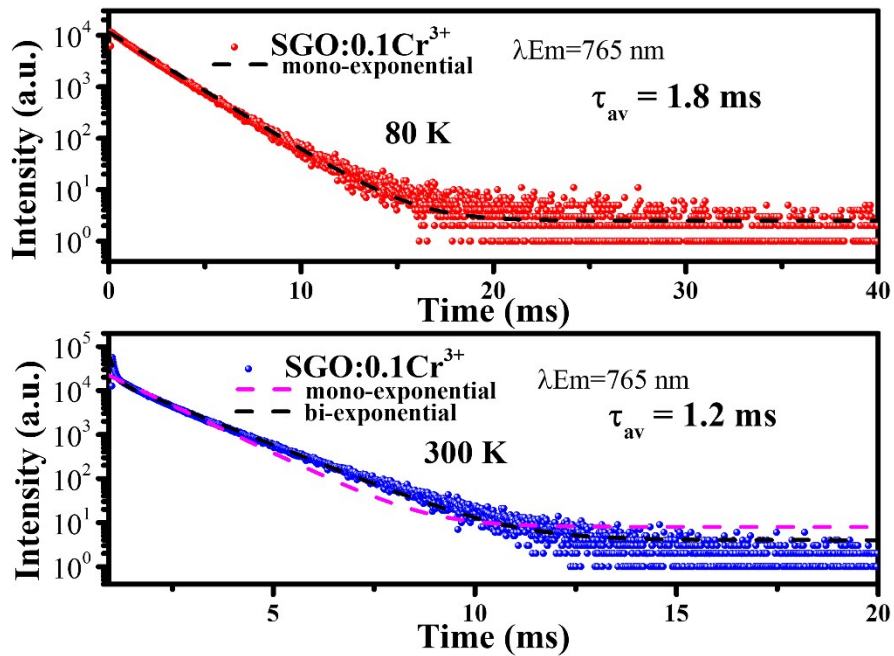


Figure S5. luminescence decay curves and multi-exponential fitting of $\text{SrGa}_{12}\text{O}_{19}:0.1\text{Cr}^{3+}$ at 80 and 300 K.

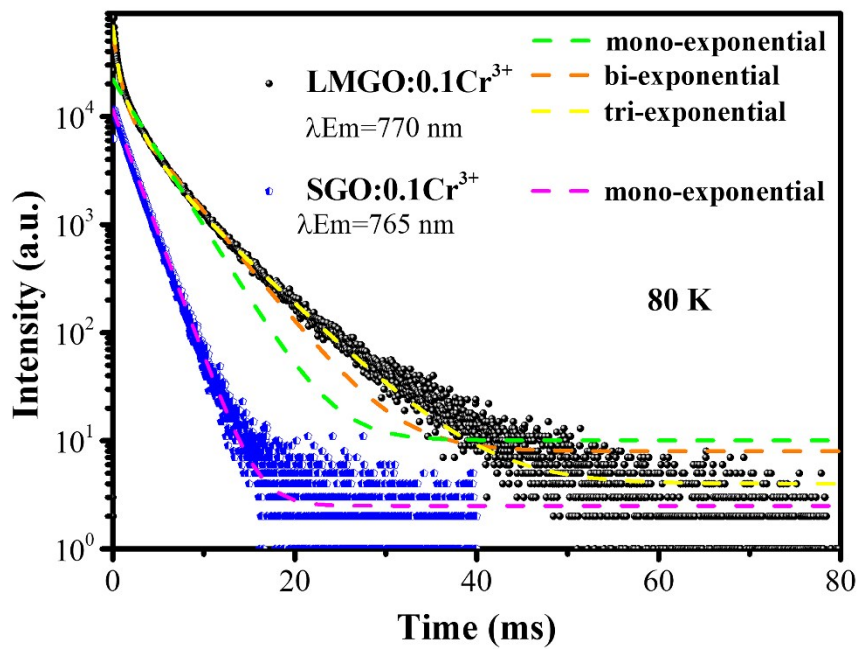


Figure S6. luminescence decay curves for $\text{LaMgGa}_{10.9}\text{O}_{19}:0.1\text{Cr}^{3+}$ and $\text{SrGa}_{11.9}\text{O}_{19}:0.1\text{Cr}^{3+}$, and multi-exponential fitting results at 80 K.

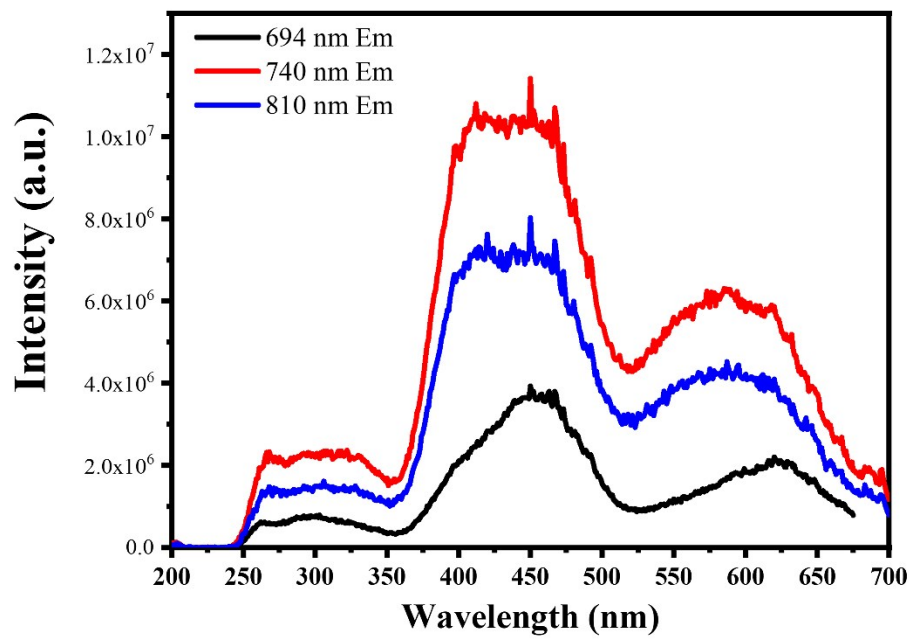


Figure S7. PLE spectra of SGO:0.1Cr³⁺ monitoring at different emission wavelength (694, 740, 810 nm).

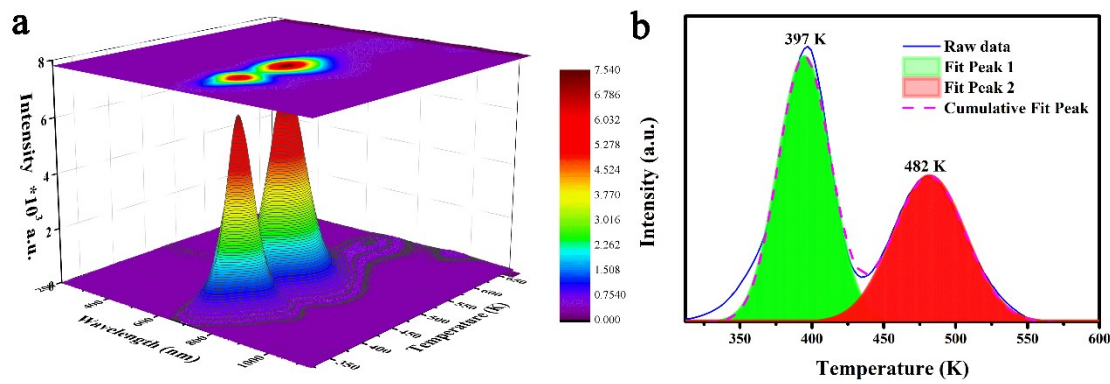


Figure S8. (a) 3D-TL curves for SGO:0.1Cr³⁺. The x and y axes denote the temperature (K) and emission wavelength (nm), respectively. (b) 2D-TL curve for SGO:0.1Cr³⁺ and Gaussian fitting curves.

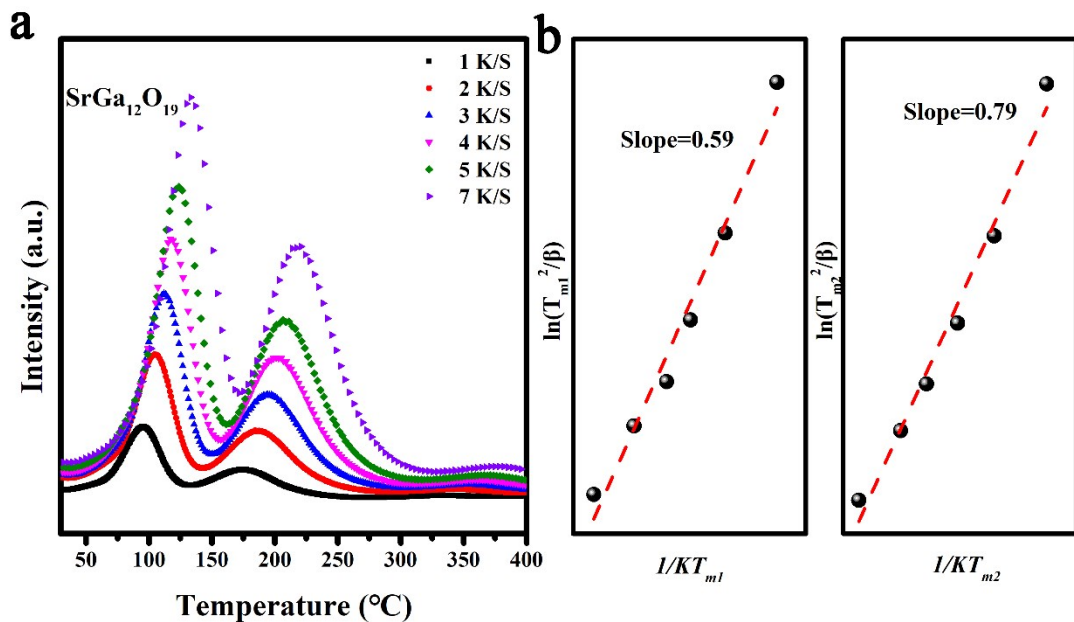


Figure S9. (a) 2D-thermoluminescence curves of $\text{SrGa}_{12}\text{O}_{19}:0.1\text{Cr}^{3+}$ via tunable heating rate β ($\beta=1, 2, 3, 4, 5, 7 \text{ K/s}$) approach. (b) $\ln(T_m^2/\beta)$ versus $1/kT_m$ scatter and linear fitting results.

References:

- [1] L. Yao, Q. Shao, S. Han, C. Liang, J. He, J. Jiang, Enhancing Near-Infrared Photoluminescence Intensity and Spectral Properties in Yb^{3+} Codoped $\text{LiScP}_2\text{O}_7:\text{Cr}^{3+}$, *Chem. Mater.* 2020, 32, 2430–2439.
- [2] T. Gao, W. Zhuang, R. Liu, Y. Liu, C. Yan, X. Chen, Design of a Broadband NIR Phosphor for Security-Monitoring LEDs: Tunable Photoluminescence Properties and Enhanced Thermal Stability, *Cryst. Growth Des.* 2020, 20, 3851–3860.
- [3] M.-H. Fang, P.-Y. Huang, Z. Bao, N. Majewska, T. Leśniewski, S. Mahlik, M. Grinberg, G. Leniec, S.M. Kaczmarek, C.-W. Yang, K.-M. Lu, H.-S. Sheu, R.-S. Liu, Penetrating Biological Tissue Using Light-Emitting Diodes with a Highly Efficient Near-Infrared $\text{ScBO}_3:\text{Cr}^{3+}$ Phosphor, *Chem. Mater.* 2020, 32, 2166–2171.
- [4] H. Zeng, T. Zhou, L. Wang, R.-J. Xie, Two-Site Occupation for Exploring Ultra-Broadband Near-Infrared Phosphor—Double-Perovskite $\text{La}_2\text{MgZrO}_6:\text{Cr}^{3+}$, *Chem. Mater.* 2019, 31, 5245–5253.
- [5] L. Zhang, S. Zhang, Z. Hao, X. Zhang, G.H. Pan, Y. Luo, H. Wu, J. Zhang, A high efficiency broad-band near-infrared $\text{Ca}_2\text{LuZr}_2\text{Al}_3\text{O}_{12}:\text{Cr}^{3+}$ garnet phosphor for blue LED chips, *J. Mater. Chem. C* 2018, 6, 4967.
- [6] B. Bai, P. Dang, D. Huang, H. Lian, J. Lin, Broadband Near-Infrared Emitting $\text{Ca}_2\text{LuScGa}_2\text{Ge}_2\text{O}_{12}:\text{Cr}^{3+}$ Phosphors: Luminescence Properties and Application in Light-Emitting Diodes, *Inorg. Chem.* 2020, 59, 13481–13488.
- [7] Z. Jia, C. Yuan, Y. Liu, X.-J. Wang, P. Sun, L. Wang, H. Jiang, J. Jiang, Strategies to approach high performance in Cr^{3+} -doped phosphors for high-power NIR-LED light sources, *Light Sci. Appl.* 2020, 9, 86.
- [8] M. Mao, T. Zhou, H. Zeng, L. Wang, F. Huang, X. Tang, R.J. Xie, Broadband near-infrared (NIR) emission realized by the crystal-field engineering of $\text{Y}_{3-x}\text{Ca}_x\text{Al}_{5-x}\text{Si}_x\text{O}_{12}:\text{Cr}^{3+}$ ($x = 0\text{--}2.0$) garnet phosphors, *J. Mater. Chem. C* 2020, 8, 1981.